Electronic structure of $1T$-VSe_2

Alex Zunger*
Department of Physics and Astronomy and Materials Research Center, Northwestern University, Evanston, Illinois 60201

A. J. Freeman
Department of Physics and Astronomy, Northwestern University, Evanston, Illinois 60201 and Argonne National Laboratory, Argonne, Illinois 60439

(Received 12 July 1978; revised manuscript received 26 February 1979)

A first-principles self-consistent (non-muffin-tin) band-structure calculations on $1T$-VSe_2 is used to analyze some of the transport and optical properties. The material appears to be metallic with characteristic overlaps between the metal d-based and nonmetal p-based bands. These overlaps are found to be sensitively modulated both by the change of the (anomalously high) c/a ratio and by the sandwich height parameter z (determining the V–Se bond length). This leads to a number of interesting predictions regarding the electronic structural changes associated with the charge-density-wave instability.

I. INTRODUCTION

The origin of charge-density waves (CDW) and their relation to the observed anomalous behavior of the layered transition-metal dichalcogenides continues to be of great theoretical and experimental interest. Of the various dichalcogenides, the $1T$ family of the group-VB compounds may be among the most interesting for study because of the wide variety of phase transitions and associated anomalous properties which they exhibit.[1,2] For the $1T$-TaS_2 and $1T$-$TaSe_2$ systems the Korringa-Kohn-Rostoker (KKR) energy-band calculations of Myron and Freeman[3] gave Fermi surfaces which are very similar for both systems, having cross sections which are approximately constant in planes that are perpendicular to the z axis and which can be nested by approximately the same wave vector parallel to the ΓM direction. Using the energy-band structure and three-dimensional Fermi surface, Myron *et al.*[4] calculated accurately the generalized susceptibility $\chi(\vec{q})$, which arises from both Fermi-surface nesting and band-structure effects for bands just above and below the Fermi energy E_F. Maxima were found at those $\vec{q}$ values which correspond to the CDW nesting vectors found by Wilson *et al.*[2] Recently, Woolley and Wexler[5] determined the band structure and Fermi surface of $1T$-TaS_2, -$TaSe_2$, and -VSe_2 using the layer method for band calculations in a so-called double muffin-tin approximation to the potential.

In our recent local-density self-consistent (SC) non-muffin-tin investigations of the electronic structure and properties of the group-IVB materials $1T$-TiS_2[6] and -$TiSe_2$,[7] we found profound changes to occur relative to the results of the early non-self-consistent muffin-tin KKR results obtained previously.[8] Whereas the muffin-tin KKR results gave a semiconductor with a fundamental gap of 2.0 and 1.2 eV at Γ and a smaller indirect gap of 1.4 and ~0.5 eV between Γ and L for TiS_2 and $TiSe_2$, respectively, our self-consistent numerical basis linear combination of atomic orbitals (LCAO) method reduced the calculated direct gap in TiS_2 to 0.8 eV and the indirect gap between 0.2 and 0.3 eV. For $TiSe_2$, our SC-LCAO results showed it to be a semimetal with an indirect overlap of 0.2 eV between Γ and L—in agreement with transport[9] and angle-resolved photoemission[10] experiments. These results appear to confirm the validity of the local density functional energy-band approach for describing the electronic structure of the layered dichalcogenides.

In addition to the standard energy-band study of $TiSe_2$, we also investigated[11] the effect of internal structural changes—specifically, the effect of varying (i) the so-called sandwich height parameter z, which determines the vertical positions of the Se atoms above and below the metal plane, and (ii) the c/a ratio on the electronic structure. We found that the observed changes in the nature of the conducting state in going from the normal semimetallic to the charge-density-wave semiconducting state can be successfully modeled by variation of a single structural parameter z. Among other results, variations of this parameter in the energy-band calculations are found to transform the system from a semimetal to a semiconducting-like state characteristic of the CDW phase and to lead to a number of possibly important experimental consequences, including the effect of pressure and intercalation on the conducting properties.

As a consequence of this work on the group-IVB

systems and the interesting results obtained especially for $TiSe_2$, we decided to investigate the electronic structure of its neighboring group-VB dichalcogenide, namely, $1T$-VSe_2, which has a number of interesting and anomalous CDW and other properties.[12-20] In this paper, we report results of two sets of extensive *ab initio* theoretical studies of the electronic band structure and properties of $1T$-VSe_2, using our recently reported *self-consistent* numerical basis set LCAO method. In the first, we discuss some of the resulting electronic properties using results determined with the observed lattice parameters. We compare the band-structure results with the non-self-consistent results of Woolley and Wexler[5] and then use them to discuss the optical, appearance potential, x-ray absorption and photoemission measurements. We also compare results obtained here for VSe_2 with its isoelectronic counterpart $TaSe_2$ and with the IVB systems $1T$-TiS_2 and $TiSe_2$. In the second part, we report a study of the variation of the electronic band structure and properties (notably, the CDW) with variation of several structural parameters: (i) the sandwich height parameter z, and (ii) the c/a ratio, which is anomalously high relative to other $1T$ compounds.[14]

II. METHODOLOGY

The self-consistent numerical basis set LCAO method[6,21] has a number of important features which are especially applicable to studies of transition-metal compounds such as $1T$-VSe_2. It uses an accurate nonlinearly optimized atomic basis set for all core, valence, and some virtual states of the atoms in the unit cell; all Hamiltonian interaction and overlap integrals are evaluated accurately using a three-dimensional numerical Diophantine integration scheme[21,22]; full self-consistency is obtained in a scheme that does not restrict the form of the crystalline charge density to any particular shape (viz, cellular or muffin-tin schemes that spherically average the charge density around each site before the next iteration is attempted). All non-muffin-tin contributions to the potential are fully retained and the electron local-density correlation functional[23] is treated as an intrinsic part of the crystal potential.

We start with an initial guess for the charge density in the form of a population-dependent superposition density $\rho_{\rm sup}(\vec{r})=\sum_{m,\alpha}\rho_\alpha(\vec{r}-\vec{R}_m)$ made up from the α'th site atomic (or ionic) charge densities $\rho_\alpha(\vec{r})$ at the lattice points $\vec{R}_m$. The single-site densities $\rho_\alpha(\vec{r})$ are obtained from self-consistent (spherically symmetric) numerical solutions of the local-density single-particle equation for the α'th atom (or ion), assuming trial occupation numbers f_{nl}^α for the corresponding atomic orbitals, leading to possible non-neutral species when $Q_\alpha = Z_\alpha - \sum_{nl} f_{nl}^\alpha \neq 0$. These occupation numbers and charges are used below as variational parameters to define an optimal superposition density. Using the initial charge density $\rho_{\rm sup}(\vec{r})$, the crystal potential $V[\rho_{\rm sup}(\vec{r})]$ is constructed, including Coulomb, exchange, and correlation contributions.[23]

The atomic basis functions $\chi_\mu^\alpha(\vec{r})$ consist of an extended numerical basis set of $\mu = 1s$ to $3d$, $4s$, and $4p$ for V and $1s$ to $4p$ and $4d$ for Se. These are obtained by solving self-consistently for the isolated V^{+Q} and $Se^{-Q/2}$ species a local-density one-particle equation similar to that used to generate the one-site densities $\rho_\alpha(r)$ but with an added external potential well that acts to suppress the long tails of the virtual atomic orbitals that might cause linear dependence in the Bloch basis set. The radius of this well is chosen so that all core orbitals will be practically unchanged by its presence. The corresponding basic Bloch set $\{\Phi_{\mu\alpha}(\vec{k},\vec{r})\}$ obtained in this way is fully defined by the assumed population and charges $\{f_{nl}^\alpha, Q^\alpha\}$, the crystal structure, and the atomic numbers Z_α; a real-space cutoff distance of 21 a.u. is required for 4-mRy accuracy.

The Hamiltonian and overlap matrix elements given in the Bloch basis $\langle\Phi_{\mu\alpha}(\vec{k},\vec{r})\,|\,\hat{0}\,|\,\Phi_{\nu\beta}(\vec{k},\vec{r})\rangle$, where $\hat{0}=1$ and $\hat{0}=V[\rho(\vec{r})]$, respectively, are calculated directly by a three-dimensional Diophantine numerical integration scheme.[21,22] (About 5000 integration points were required to obtain an accuracy of 1–3 mRy in the valence and lowest nine conduction bands and ~18-mRy accuracy in the core bands.) All the multicenter integrations encountered in conventional LCAO theory are completely avoided, and any general form of the crystal potential or basis set can be treated equally in a straightforward manner.

The secular equation is solved for a set of wave vectors $\{\vec{k}_q\}$ in the irreducible section of the Brillouin zone (BZ) (see notation in Fig. 1) and the resulting wave functions $\{\psi(\vec{k}_q,\vec{r})\}$ for all occupied bands are used to compute the crystal density, but with the BZ integration replaced by a discrete summation over the set $\{\vec{k}_p=\Gamma,M,K,A,L,H\}$

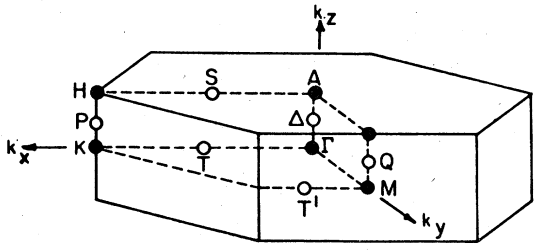

FIG. 1. Brillouin zone for $1T$-VSe_2.

with their associated nearest-volume weights, i.e., $w(\vec{k}_\rho)$:

$$\rho_{cry}(\vec{r}) = \sum_{\vec{k}_\rho} w(\vec{k}_\rho) \sum_{j=1}^{\sigma_{oc}} \psi_j^*(\vec{k}_\rho, \vec{r}) \psi_j(\vec{k}_\rho, \vec{r}) , \qquad (1)$$

where j denotes the band index and extends to all σ_{oc} occupied bands below the Fermi energy. This variational charge density is in general not equal to the starting superposition density on two counts: (i) self-consistency is not achieved as yet, and (ii) in general, there are parts of the multicenter variational density of form (1) that are not describable by any superposition density which assumes spherical (overlapping) auxiliary functions $\rho_\alpha(\vec{r} - \vec{R}_m)$ centered only on atomic sites. We hence proceed to a two-stage self-consistency. In the first stage, we vary the atomiclike occupation numbers f_{nl}^α and charges Q_α (computing for each such set the Bloch basis functions $\Phi_{\mu\alpha}(\vec{k}, \vec{r})$, the new superposition density $\rho_{sup}(\vec{r}, \{f_{nl}^\alpha, Q^\alpha\})$, the corresponding crystal potential, and the resulting variational density $\rho_{cry}(\vec{r})$ so as to minimize, in the least-squares sense, the deviation $\Delta\rho(\vec{r}) \equiv \rho_{cry}(\vec{r}) - \rho_{sup}(\vec{r})$ over the unit-cell volume. This yields the "best" single-site atomic configuration for the superposition representation of the variational charge density.

However, as noted in (ii), this superposition representation cannot account for the full anisotropy of the charge density in a covalently bonded material and hence, $\Delta\rho(\vec{r})$ cannot be reduced to zero (or a constant) even by nonlinear optimization processes such as we employ. Hence we proceed in stage 2 to full self-consistency by treating the *residual* charge-density difference $\tilde{\Delta}\rho(\vec{r})$ (i.e., that resulting from the last iteration of stage 1 in the self-consistency) beyond the superposition representation. This can be done either by using real-space techniques that project $\tilde{\Delta}\rho(\vec{r})$ onto some multicenter basis set (e.g., atom plus bond-centered Gaussians)[24] or by reciprocal space techniques in which $\tilde{\Delta}\rho(\vec{r})$ is expanded in symmetrized plane waves.[24] In both cases (and in the mixed-representation technique), one uses the analytic representation of $\tilde{\Delta}\rho(\vec{r})$ to solve the associated Poisson equation and obtain the correction to the interelectronic Coulomb potential and the modified exchange potential $V_x[\rho_{sup}(\vec{r}) + \tilde{\Delta}\rho(\vec{r})]$ needed to proceed to full self-consistency. We find, in the case of a partially covalently bonded material such as VSe_2, that the residual density $\tilde{\Delta}\rho(\vec{r})$ tends to delocalize smoothly over large parts of the unit-cell volume (e.g., the antibond sites as well as the bond regions) with no obvious localization centers and hence an expansion in terms of symmetrized plane waves is both efficient and accurate. Note that unlike the methods that employ a plane-wave basis set for valence-band calculations in a solid (e.g., the pseudopotential approach), we do not face the convergence problems associated with a Fourier expansion of the *total* valence densities, and instead, only the relatively smooth part, $\tilde{\Delta}\rho(\vec{r})$, has to be treated. In this context, a careful selection of the electron configuration becomes of practical importance; stage 1 of self-consistency produces not only a nearly SC result, but also results in a spatially smooth $\tilde{\Delta}\rho(\vec{r})$ [by absorbing all localized features of $\rho_{cry}(\vec{r})$ into the superposition density] which is readily amenable to a rapidly convergent Fourier representation. The iterative calculation of $\rho(\vec{r})$ requires the determination of the Fermi energy. This is done approximately (at each iteration) using six $\vec{k}$ points. At the self-consistency limit we have verified the accuracy of this determination (0.05 eV) by using a grid of 24 $\vec{k}$ points.

III. RESULTS

A. Energy band structure

Figure 2 shows the self-consistent band structure of 1T-VSe_2. We find a lower valence band (VB2 at 12.3–14.3 eV below the Fermi energy E_F) that is composed predominantly of Se 4s orbitals and is separated from the upper valence band (VB1) by a 5.89-eV gap. This upper valence band is about 5.80 eV wide and is composed of bonding combinations of σ-type Se 4p orbitals with some admixture of V 3d and 4p character. The antibonding σ^*-type counterpart ($CB3$) of this band lies (by, e.g. 7.3 eV at Γ) above $VB1$. In this large bonding-antibonding gap, one finds the metal d-based bands. The lower part of this band ($CB1$) is about 2 eV wide and is ligand-field split at Γ and A into two components: the singly degenerate $\Gamma_{1,c}^+$ and $A_{1,c}^+$ pair and the doubly degenerate $\Gamma_{3,c}^+$ and $A_{3,c}^+$ pair with $\Gamma_{1,c}^+$ ($A_{1,c}^+$) lying below (above) the $\Gamma_{3,c}^+$ ($A_{3,c}^+$) level. The second component of the metal d-based band ($CB2$) is slightly narrower than $CB1$ and has a center of gravity hybridization gap ($CB1$-$CB2$) of 1.7 eV; the lower d-based band overlaps the Se p-based band by 0.71 eV at L, 0.47 eV at M, and 0.40 eV at A (shaded areas below E_F in Fig. 2).

The Fermi energy lies in the lower part of the $CB1$ band at −7.05 eV below vacuum and forms hole surfaces around K, H, and P (dashed areas above E_F in Fig. 2) and electron surfaces around M, L, and Q. The electron surface in the Γ-K-M plane occupies 0.45 of the MK line, 0.51 of the ΓK line, and the entire ΓM line, while on the parallel A-H-L plane it extends to about 0.6 of the LA

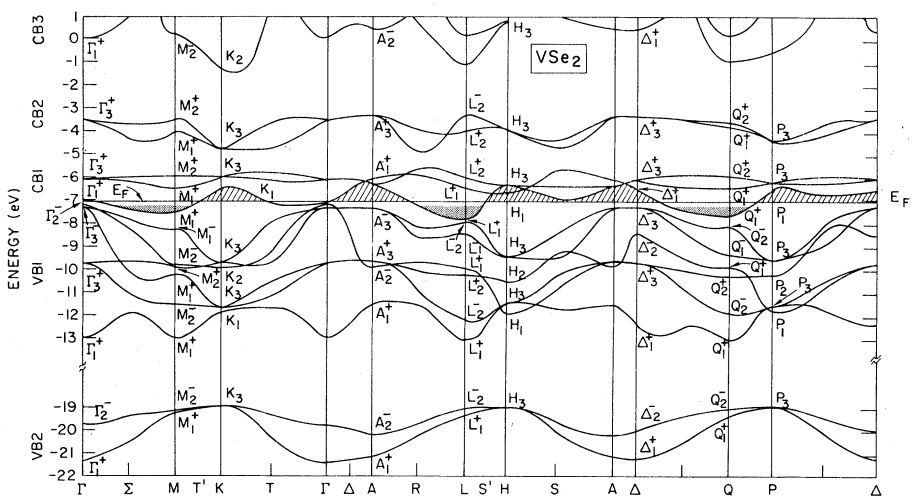

FIG. 2. Exchange and correlation self-consistent band structure of 1 T-VSe_2. The dotted area indicate regions of overlap of the d-based band with the p-based bands; stripped areas indicate hole surfaces. $VB2$, $VB1$, and $CB3$ denote the Se s-like valence band, Se p-like band, and the anti-bonding conduction bands, respectively. $CB1$ and $CB2$ refer to the two components of the d-based conduction band. Note the change of scale between $VB1$ and $BV2$.

line, 0.3 of the LH line, and does not occur along the AH line. This topology is similar to that found in 1T-$TaSe_2$.[4] Due to the pronounced dispersion of the lowest d-based band along $\Gamma^+_{1,c} - A^+_{1,c}$ and $\Delta^+_{1,c} - Q^+_{1,c}$ (due to interlayer interaction) and the $M^+_{1,c} - K_{1,c}$ and $A^+_{3,c} - L^+_{1,c}$ bands, E_F is expected to occur in a region of relatively low density of states while at slightly lower energies the density of states is expected to increase, due to the occurrence of the flat pieces of the bands at $M^+_{1,c}$ and $L^+_{1,c}$. The bands are symmetric along the L-M-L' and M-K-H' lines with respect to the M-K line, while they show a pronounced asymmetry (0.1–0.4 eV) along the interior of these lines. Similar effects have been studied in our previous calculation on $TiSe_2$.[7]

Our band structure is in overall qualitative agreement with the muffin-tin non-self-consistent study by Woolley *et al.*[5] One notes, however, a few differences such as the different order of valence bands at Γ (the top of the valence band in their calculation is the $\Gamma^-_{3,v}$ level, which lies about 0.8 eV above $\Gamma^-_{2,v}$, while in our calculation $\Gamma^-_{2,v}$ forms the top of the band) and at H ($H_{3,v}$ and $H_{1,v}$ are interchanged). In addition, their band *overlaps* are about a factor of 3–4 times smaller than our values. We have found the same differences in comparing our *non*-muffin-tin calculations on 1T-TiS_2[6] and 1T-$TiSe_2$[7] with previous muffin-tin calculations.[3,4,8] We further note that the occurrence of a $\Gamma^-_{3,v}$ valence band which is well separated from the $\Gamma^-_{2,v}$ level in the calculation of Woolley *et al.*[5] is inconsistent with the absence of the "α" photoemission line in this material.[12] By contrast, our band model predicts that the $\Gamma^-_{2,v}$ and $\Gamma^-_{3,v}$ levels form a single $\alpha+\beta$ line which is about $\frac{3}{2}$ times stronger than the $\Gamma^+_{3,v}$ γ line, in qualitative agreement with photoemission data. We find a similar situation to occur in TiS_2 which is also characterized by a $\Gamma^-_{2,v}$-type valence band edge and shows only two pronounced photoemission peaks.[12]

B. Comparison of trends in results for VSe_2 with those for TiS_2 and $TiSe_2$

The general pattern of the bands in VSe_2 is qualitatively similar to that previously obtained by us for TiS_2[6] and $TiSe_2$.[7] There are, however, some important differences in the electronic structure of these compounds. Table I summarizes some of the pertinent gaps in these materials. One first notes that all the p/d gaps at Γ, M, and L (both direct and indirect) decrease monotonically as one goes from TiS_2 to $TiSe_2$ and VSe_2. This is consistent with the decrease in ionicity (Pauling's electronegativity differences between the metal and nonmetal atoms being 1.0, 0.9, and 0.8 for TiS_2, $TiSe_2$, and VSe_2, respectively) and the increase in covalent character along this series. It is also in line with the observation of Greenaway and Nitsche[25] that the energy of the prominent peaks in the reflection spectra of transition-metal dichalcogenides in the $VB1$-$CB1$ and $VB1$-$CB2$ region increases with the ionic character of the constituent atoms.

Perhaps of even greater significance is the increase in the basic bonding-antibonding gap ($CB3$-$VB1$): the values at the Γ point are 6.0, 6.7, and 7.3 eV for TiS_2, $TiSe_2$, and VSe_2, respectively. This gap monitors the strength of the orbital interaction within the Se/S p and Ti/V s and p manifold, and forms a strong indication of an advanced covalent bond in VSe_2. This basic gap is reflected in the absorption spectra[25,26] of these materials as a pronounced window at around 6–8 eV, and is totally absent in the Zr and Hf compounds,[26] which are significantly more ionic. Hence we suggest that the decrease in the chalcogen p-based and

TABLE I. Comparison of bandwidths and major gaps between the chalcogen p-like and metal d-like bands (denoted by an asterisk) in TiS_2, $TiSe_2$, and VSe_2. Results are given in eV.

Quantity	TiS_2 [a]	$TiSe_2$ [b]	VSe_2
width of $VB1$	5.49	5.70	5.80
width of $VB2$	1.94	2.00	2.41
$VB1$-$VB2$ gap	6.76	6.92	5.98
σ-σ^* gap [$CB3$-$VB1$]	6.0	6.7	7.3
$CB1$-$CB2$ splitting	2.3	2.1	1.7
p/d gaps			
$\Gamma\Gamma^*$	0.84	0.32	0.20
MM^*	2.51	2.04	0.77
LL^*	1.63	1.32	0.05
ΓM^*	0.29	0.12	−0.47
ΓL^*	0.23	−0.20	−0.71
edge of $VB1$	$\Gamma_{2,v}^-$	$\Gamma_{3,v}^-$	$\Gamma_{2,v}^-$

[a] Reference 6.
[b] Reference 7.

metal d-based gaps and the increase in the bonding-antibonding gaps form a reliable criteria for the degree of covalency in these materials.

Similarly, we find that the widths of the fundamental valence bands ($VB1$ and $VB2$ in Table I are substantially larger in VSe_2 than in TiS_2 and $TiSe_2$ in accord with the greater covalent character of the former. The gap between the two components of the valence band, $VB1$ and $VB2$, reflects the basic s to p atomic promotion energy on the chalcogen, modified by solid-state effects. Hence, the $VB1$-$VB2$ gap in TiS_2 is about 0.16 eV smaller than the corresponding gap in $TiSe_2$, in accord with the smaller s-p gap in S relative to Se (≈0.16 eV in the free atoms, using the same exchange and correlation functionals employed in the band calculation). The corresponding gap in VSe_2 (5.98 eV) is substantially smaller than the value expected from the selenide s to p promotion energy. This band-gap narrowing again reflects the enhancement in covalent character which results in an increased s/p hybridization on Se.

We note that the center-of-gravity splitting of the $CB1$-$CB2$ hybridization gap is rather similar in TiS_2 and $TiSe_2$ (2.3 and 2.1 eV, respectively), in good quantitative agreement with the interpretation of the appearance potential data of Webb and Williams,[13] and the x-ray absorption spectra of Fischer[27]; this gap is significantly narrower in VSe_2 (1.7 eV), a value that is more characteristic of trigonal-prismatic structures.[1,25,26] The opposite behavior is seen in the splitting of the lowest conduction bands at Γ: the $\Gamma_{1,c}^+ - \Gamma_{3,c}^+$ gap is 0.42 and 0.38 eV for TiS_2 and $TiSe_2$ and 0.93 eV for VSe_2. Again, this large splitting is characteristic of trigonal prismatic structures.[1,25,26] Indeed, photoemission studies of Shepherd and Williams[12] indicated that the emission line from the occupied part of the d band is of comparable width in 1T-VSe_2 and in the trigonal prismatic 2H-$NbSe_2$ structure despite the substantial differences in the total $CB1+CB2$ width in these materials. Hence, the magnitude of the p/d band overlap, the hybridization gap ($CB1$-$CB2$), and the ligand-field gap is determined by the site symmetry of the metal ion, and both 1T and 2H compounds having similarly high c/a values can be characterized by substantial band overlap and a large splitting between the components of the lower conduction band. Thus it would seem that 1T-VSe_2, with its abnormally large c/a ratio (1.817 compared with 1.671 and 1.697 for TiS_2 and $TiSe_2$, respectively, and the value of 1.633 for ideal octahedral packing), has a d-band structure more characteristic of the 2H trigonal prismatic structures (c/a values of 1.85–1.82). Indeed, the simple Hückel model of Huisman *et al.*[28] demonstrates that the splitting of the "t_{2g}" state at the bottom of $CB1$ (e.g., $\Gamma_{1,c}^+$ and $\Gamma_{3,c}^+$) equals $-\frac{1}{2}\Delta$ for the ideal octahedral structure, where Δ is the d-p_σ gap, while for trigonally distorted systems the splitting increases with $V_{\sigma d}/\Delta$, where $V_{\sigma d}$ is the matrix element coupling d and p_σ states. Note that this "ligand-field" splitting between the d_{z^2} and the $d_{xy}+d_{x^2-y^2}$ components increases with the strength of the point-ion field for systems which otherwise have similar octahedral fields (e.g., TiS_2 has a somewhat larger splitting than $TiSe_2$ which has a similar c/a ratio), while a different source of variation in this gap stems from substantial deviations from the octahedral field (e.g., VSe_2 with its distorted octahedral structure having a much larger gap).

It is interesting to compare the band structure of the isoelectronic group-V materials 1T-$TaSe_2$[4] and 1T-VSe_2. In contrast with the corresponding group-IV systems ($TiSe_2$ and $HfSe_2$) in which the Fermi energy intersects the p/d region, the group-V materials have their E_F in the lower d-based conduction band, which accommodates a single electron. There is, however, a significant difference between the Ta and V compounds; while the d-based band in $TaSe_2$ is separated by a large gap (~0.1 Ry) from the chalcogen p-based valence band, the d-based band overlaps significantly the p band in the more covalent VSe_2 system. The formation of this large gap is consistent with the increased ionic character of both TaS_2, and $TaSe_2$ and is also evident from the occurrence of the basic bonding-antibonding gap at a much lower energy (cf., in the reflectivity spectra of Manig *et al.*[19]).

The strong p/d hybridization is expected to give rise to a more complicated pattern of the Fermi-

surface-driven instabilities in that $1T$-VSe_2 can exhibit not only a nesting of electron and hole pieces *inside* the d-based bands with wave vectors parallel to the ΓM directions as found in $1T$-$TaSe_2$,[4] but an additional nesting of electron-hole surfaces can occur between the d-based conduction band and the p-based valence band, respectively. We expect the latter mechanism to depend sensitively on the structural parameters which determine the overlap of the conduction and valence bands.

Measurements of the magnetic susceptibility and electrical resistivity of the iron-doped system $V_{1-x}Fe_xSe_2$[15] furnish indirect evidence for the p/d band overlap in VSe_2. The iron, which substitutionally occupies the V sites in the VSe_2 lattice and thus shows no extra x-ray diffraction lines, is found to be divalent.[15] Hence, charge neutrality requires that the vanadium valency N_v be $(4-2x)/(1-x)$, if one assumes Se to be divalent. For $x=\frac{1}{3}$, this means that vanadium reaches a maximum valency of $N_v=5$ and thus one expects no further substitution beyond this limit if the mobile electrons are extracted solely from the metal sublattice. However, due to the overlap of the V-based d band with the Se-based p band, further substitution is possible, leading to hole formation on the Se sublattice. This hole formation is expected to occur, on the basis of our band structure, even for $x<\frac{1}{3}$ due to the significant admixture of Se character into the metal d-based bands (e.g., at $K_{3,c}$ and $H_{3,c}$).

The substitution of iron is expected to reduce the dimensions of the electron surfaces in the lower conduction band (which would eventually contain electrons only near the minima at $L^+_{1,c}$ and $M^+_{1,c}$), and to decrease thereby the length of the corresponding wave vector necessary to span the electron and hole pieces. In turn, this is expected to reduce the instability transition temperature, as is indeed observed ($T\approx 0$ for $x=0.035$). However, one cannot separate this effect from that caused by the random fluctuations introduced in the metal potential, and indeed, even substitution of Ti (which is closer in its valency to V than Fe) was shown to rapidly suppress the transition ($T_0\approx 0$ for $x=0.04$).[15]

C. Dependence of band structure and properties on structural parameters

In order to elucidate the effects of the structural parameters of $1T$-VSe_2 on its electronic properties, we undertook two studies: in the first, we vary (at constant c/a) the "sandwich height parameter" z which determines the vertical positions of the Se atoms above and below the metal plane. While its precise value for VSe_2 is not known experimentally, it is close to the ideal octahedral value of $\frac{1}{4}$[9,26] in both TiS_2 and $TiSe_2$. In the second study, we try to understand the effects of the variations in the c/a ratio on the electronic structure. This is motivated by the fact that VSe_2 is characterized by an anomalously large c/a ratio relative to the other $1T$ compounds.[14] However, since the a-lattice parameter is rather similar in TiS_2, $TiSe_2$, and VSe_2, we vary c/a by only changing c. Clearly, the actual atomic displacements that accompany the CDW are much more complex than the above model (e.g., in $TiSe_2$ the new unit cell contains eight molecules!). What we are attempting here is to isolate the effects of two crucial structural variables that modulate the elementary interatomic separation, preserving for simplicity the crystal structure.

1. Variation with sandwich height parameter z

Figure 3 shows the variation in some band eigenvalues at high symmetry points in the zone with the sandwich height parameter z; Fig. 4 depicts the variations in the p/d band overlaps at Γ and L, M with z. The cross-hatched area in Fig. 3 represents the band overlap between the highest valence band at Γ ($\Gamma^-_{2,v}$ and $\Gamma^-_{3,v}$) and lowest conduction band at M ($M^+_{1,c}$), while the dotted area represents the extra overlap produced at $L^+_{1,c}$. It is seen that for small z values the bonding $\Gamma^-_{3,v}$ level dips down below the bottom of the conduction band at $M^+_{1,c}$ leading to a finite $\Gamma^-_{3,v}-M^+_{1,c}$ gap, while for larger z values, $\Gamma^-_{3,v}$ is destabilized and leads to a significant band overlap which reaches a maximum at $z=0.28$. Similar behavior characterized the $\Gamma^-_{3,v}-L^+_{1,c}$, $\Gamma^-_{2,v}-M^+_{1,c}$, and $\Gamma_{2,v}-M^+_{1,c}$ bands with the maximum band overlap occurring at widely different z values. Note that while the p_π-type bonding $\Gamma^-_{2,v}$ level forms the upper edge of the valence band for $z\leq 0.256$, it interchanges position with the p_σ-type bonding $\Gamma^-_{3,v}$ level for $z>0.260$. Qualitatively similar trends have been observed in our previous studies on $TiSe_2$[7]; however, due to the substantially larger band overlap which occurs in VSe_2, we do not find a z value in the range studied, which causes *all* band overlaps to disappear and to lead to a semiconducting-like state. In $TiSe_2$ one can model the observed decrease in magnetic susceptibility and increase in electrical resistivity upon CDW formation[11] in terms of a substantial shortening of some of the Ti-Se bonds (e.g., an effective shortening of z relative to its normal phase value). This is caused by coupling of the electron states at L (localized predominantly on the Ti site) and the hole states at Γ (localized predominantly on the Se sites) mediated by a zone-boundary phonon. It appears

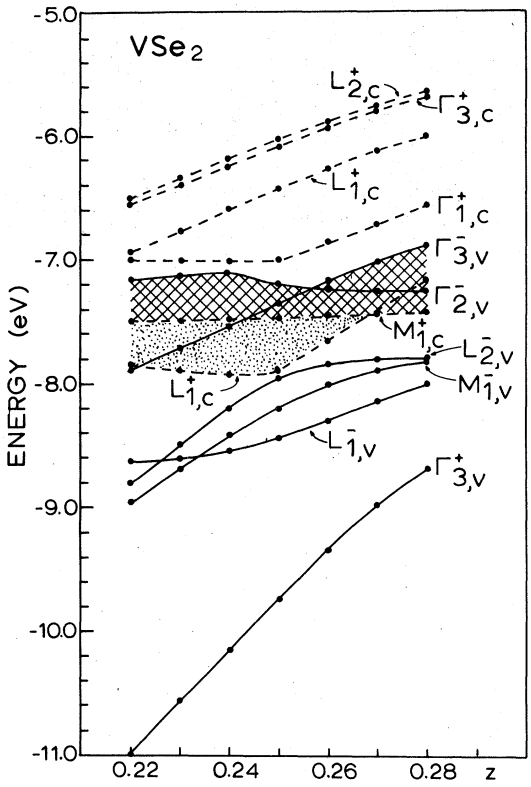

FIG. 3. Variation of high-symmetry band energies in 1T-VSe_2 with the sandwich height parameter z. The dotted area indicates the d/p band overlap at L, while the cross-hatched area denotes a similar overlap at M. Full lines and dashed lines denote valence and conduction bands, respectively. The full dots indicate calculated points.

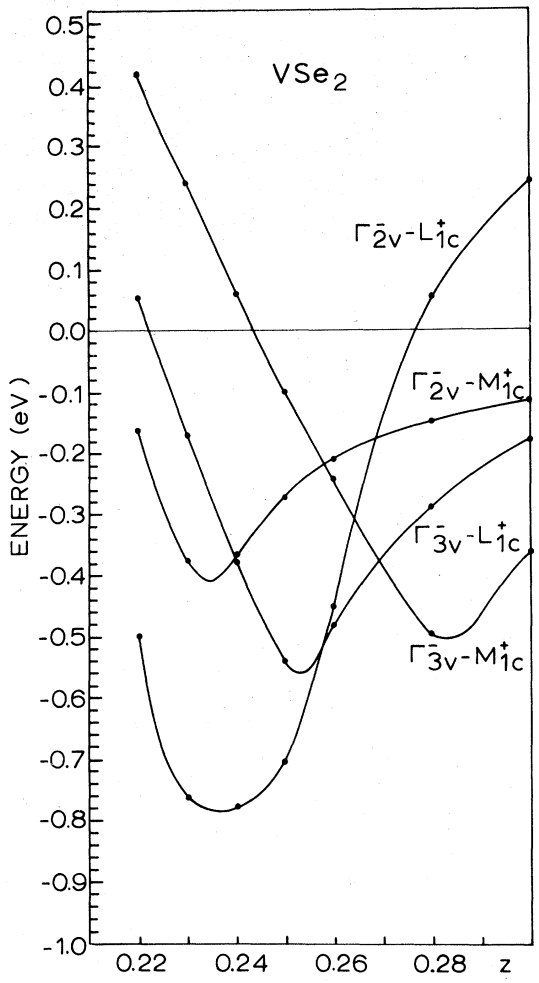

FIG. 4. Variation of some energy gaps at 1T-VSe_2, with the sandwich height parameter z.

unlikely that a similar mechanism prevails in VSe_2. The observed decrease in the magnetic susceptibility and the increase in the electrical resistivity upon CDW formation in 1T-VSe_2[10,15] is consistent with a much lower loss in Fermi-surface area (~30%) than in the analogous transition in 1T-$TiSe_2$.[9]

2. *Variation with c/a values*

The dependence of selected band eigenvalues at Γ, L, M, and A on the c/a value is depicted in Fig. 5. The p/d band overlap is seen to change considerably with the c/a ratio: both the overlap at M ($M^+_{1,c}$ with either $\Gamma^-_{2,v}-\Gamma^-_{3,v}$, displayed as the dotted area) and at L ($L^+_{1,c}$ with $\Gamma^-_{2,v}$ or $\Gamma^-_{3,v}$, displayed as the dotted plus cross-hatched areas) decrease as c/a increases. At the same time, the splitting of the lowest d-based conduction band at Γ ($\Gamma^+_{1,c}-\Gamma^+_{3,c}$, shown as the dashed area) increases considerably, the lowest singly degenerate $\Gamma^+_{1,c}$ component decreases in energy and the upper doubly degenerate representation $\Gamma^+_{3,c}$ increases. Hence, as c/a increases, the occupation of the d-based conduction band around Γ increases at the expense of reducing the volume of the electron surfaces around L and M. If one conceives of the Fermi-surface instability leading to the CDW state as being due to nesting of the electron-hole surfaces within the d-based band with a typical spanning vector $\vec{q}\|\Gamma M$ or $\vec{q}\|\Gamma K$, this suggests that relatively small changes in the c/a ratio would drastically change the magnitude of the appropriate spanning vector, modifying thereby the coupling mechanism and the transition temperature. In this model, the rapid lowering of the conduction band at Γ relative to the edge of the p-based valence-band and to the conduction-band minima at L and M, suggests that the CDW instability would occur over a rather limited c/a range. Thus if one were to decrease the c/a ratio, either by chemical substitution that would reduce the covalency of the system (without neces-

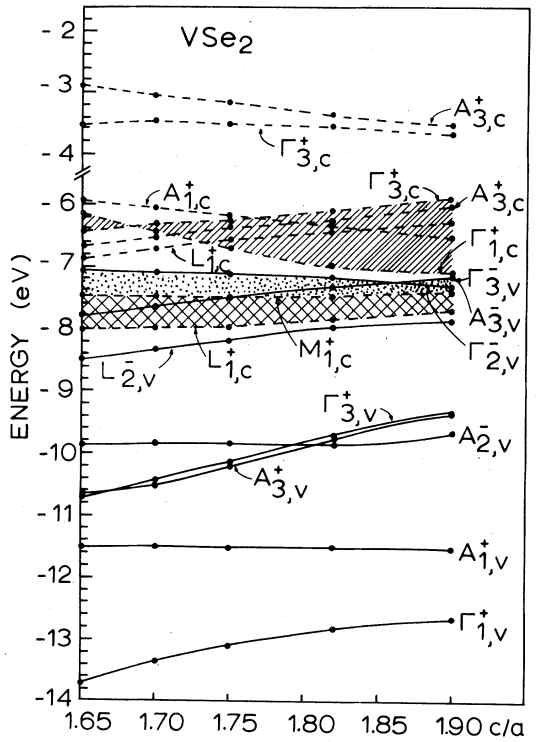

FIG. 5. Variations in some high-symmetry band eigenvalues at $1T$-VSe_2 with the c/a ratio.

sarily depopulating the d bands) or by external means, notably pressure, this model predicts a suppression of the CDW instability. Note that due to the complete decoupling of the p-based valence band from the d-based conduction band in the tantalum dichalcogenides, one does not expect that changes in the c/a value would drastically affect the instability temperature.

One further notes that the magnitude of the $\Gamma^+_{1,c} - \Gamma^+_{3,c}$ splitting of the "t_{2g}"-type conduction-band state is not dictated by the metal site symmetry but rather by the c/a ratio. Although the trigonal prismatic $2H$ compounds are usually characterized by a larger splitting than the corresponding octahedral $1T$ compounds, it is apparently possible to stabilize covalently a $1T$ compound with a large c/a ratio and produce a large $\Gamma^+_{1,c} - \Gamma^+_{3,c}$ gap. At low c/a values, the singly degenerate $\Gamma^+_{1,c}$ component destabilizes relative to the doubly degenerate $\Gamma^+_{3,c}$ component, and their order can eventually be interchanged (cf., Fig. 5). A similar interchange in $A^+_{1,c} - A^+_{3,c}$ occurs at a larger c/a value. Such an interchange is expected to alter significantly the optical reflectance and the infrared absorption spectra (cf., the $\Gamma^+_{1,c} - \Gamma^+_{3,c}$ absorption band noted by Wilson and Yoffe,[1] and the discussion of Huisman *et al.*[28] for this transition). Similarly, the hybridization gap between $CB1$ and $CB2$ decreases appreciably with increasing c/a, changing it from a value of 2.3 eV at $c/a = 1.67$ (which is similar to the values characterizing the $1T$ compounds with similar c/a ratios) to about 1.5 eV at $c/a = 1.85$ [which is more characteristic of compounds ($1T$ or $2H$) having large c/a ratios].

Finally, the data of Fig. 5 also show that some interesting trends in the dispersion of the bands along the interlayer Γ-A direction can be classified into two groups: that of the out-of-plane p_z-type representations of the pairs $\Gamma^+_{1,v} - A^+_{1,v}$ and $\Gamma^-_{2,v} - A^-_{2,v}$ and the in-plane p-type representations of $\Gamma^+_{3,v} - A^+_{3,v}$ and $\Gamma^-_{3,v} - A^-_{3,v}$. The first group shows a strong dispersion due to the pronounced p_z-p_z overlap along the interlayer direction and are hence sensitive to the magnitude of the c axis. The splitting between these corresponding pairs decreases when c increases and in the limit of infinite interlayer separation they collapse into degenerate representations. On the other hand, the p_σ-type pairs are characterized by a very low dispersion along Γ-A (the $\Gamma^+_{3,v} - A^+_{3,v}$ and $\Gamma^-_{3,v} - A^-_{3,v}$ pairs being almost degenerate) due to their low amplitude in the interlayer space, and their c-axis dependence merely reflects their dependence on the metal-chalcogen distance. The dispersion of the lowest conduction band along $\Gamma^+_{1,c} - A^+_{1,c}$ is similarly shown to increase with the c/a ratio, causing electrons to fill the regions near Γ at the expense of additional hole formation around A. This would tend to enhance the conductivity normal to the plane, as indicated by Woolley *et al.*[5]

ACKNOWLEDGMENTS

This work has been supported by the NSF under the NSF-MRL program through the Materials Research Center of Northwestern University under Grant No. DMR 76-80847, the Air Force Office of Scientific Research, under Grant No. 76-2948, and the U. S. Department of Energy.

*Present address: Solar Energy Research Institute, Golden, Colo. 80401.

[1] J. A. Wilson and A. D. Yoffe, Adv. Phys. 18, 193 (1969).
[2] J. A. Wilson, F. J. DiSalvo, and S. Mahajan, Adv. Phys. 24, 117 (1975); J. A. Wilson, Phys. Status. Solidi B 86, 11 (1978).
[3] H. W. Myron and A. J. Freeman, Phys. Rev. B 11, 2735 (1975).
[4] H. W. Myron, J. Rath, and A. J. Freeman, Phys. Rev. B 15, 885 (1977).
[5] A. M. Woolley and G. Wexler, J. Phys. C 10, 2601 (1977).

[6]A. Zunger and A. J. Freeman, Phys. Rev. B 16, 906 (1977).
[7]A. Zunger and A. J. Freeman, Phys. Rev. B 17, 1839 (1978).
[8]H. W. Myron and A. J. Freeman, Phys. Rev. B 9, 481 (1976).
[9]F. J. DiSalvo, D. E. Moncton, and J. V. Waszczak, Phys. Rev. B 14, 4321 (1976).
[10]M. M. Traum, G. Margaritondo, N. V. Smith, J. E. Rowe, and F. J. DiSalvo, Phys. Rev. B 17, 1836 (1978).
[11]A. Zunger and A. J. Freeman, Phys. Rev. Lett. 40, 1155 (1978).
[12]F. R. Shepherd and P. M. Williams, J. Phys. C 7, 4427 (1974).
[13]C. Webb and P. M. Williams, Phys. Rev. B 11, 2082 (1975).
[14]A. H. Thompson, Phys. Rev. Lett. 34, 520 (1975).
[15]F. J. DiSalvo and J. V. Waszczak, J. Phys. Colloq. 37, 157 (1976).
[16]M. Bayard and M. J. Sienko, J. Solid State Chem. 19, 325 (1976).
[17]J. E. Smith, J. C. Tsang, and M. W. Shafer, Solid State Commun. 19, 283 (1976).
[18]C. F. Van Bruggen and C. Haas, Solid State Commun. 20, 251 (1976).
[19]R. Manig, B. Thieblemont, L. Martin, and F. Pradal, Nuovo Cimento B 38, 196 (1977).
[20]A. H. Thompson and B. G. Silbernagel (unpublished).
[21]A. Zunger and A. J. Freeman, Phys. Rev. B 15, 4716 (1977).
[22]D. E. Ellis and G. S. Painter, Phys. Rev. B 2, 2887 (1970).
[23]K. S. Singwi, A. Sjölander, P. M. Tosi, and R. H. Land, Phys. Rev. B 1, 1044 (1970).
[24]T. Asada, A. Zunger, and A. J. Freeman (unpublished).
[25]D. L. Greenaway and R. Nitsche, J. Phys. Chem. Solids 26, 1445 (1965).
[26]H. P. Hughes and W. Y. Liang, J. Phys. C 10, 1075 (1977).
[27]D. W. Fischer, Phys. Rev. B 8, 3576 (1972), and references therein.
[28]R. Huisman, R. De Jonge, C. Haas, and F. Jellinek, J. Solid State Chem. 3, 56 (1971).